

Dimensionality Dependent Water Splitting Mechanisms on Free Manganese Oxide Clusters

Sandra M. Lang,[†] Irene Fleischer,[†] Thorsten M. Bernhardt,^{*,†} Robert N. Barnett,[‡] and Uzi Landman^{*,‡}

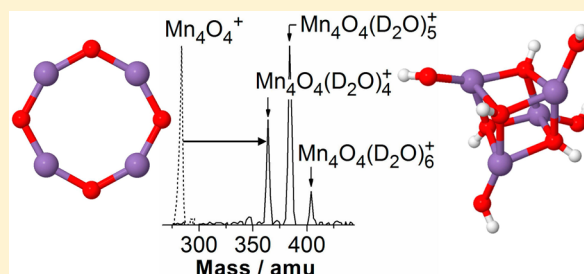
[†]Institute of Surface Chemistry and Catalysis, University of Ulm, Albert-Einstein-Allee 47, 89069 Ulm, Germany

[‡]School of Physics, Georgia Institute of Technology, Atlanta, Georgia 30332-0430, United States

S Supporting Information

ABSTRACT: The interaction of ligand-free manganese oxide nanoclusters with water is investigated, aiming at uncovering phenomena which could aid the design of artificial water-splitting molecular catalysts. Gas phase measurements in an ion trap in conjunction with first-principles calculations provide new mechanistic insight into the water splitting process mediated by bi- and tetra-nuclear singly charged manganese oxide clusters, Mn_2O_2^+ and Mn_4O_4^+ . In particular, a water-induced dimensionality change of Mn_4O_4^+ is predicted, entailing transformation from a two-dimensional ring-like ground state structure of the bare cluster to a cuboidal octa-hydroxy-complex for the hydrated one. It is further predicted that the water splitting process is facilitated by the cluster dimensionality crossover. The vibrational spectra calculated for species occurring along the predicted pathways of the reaction of Mn_4O_4^+ with water provide the impetus for future explorations, including vibrational spectroscopic experiments.

KEYWORDS: *Ab initio calculations, manganese oxide clusters, dimensionality crossover, water splitting, gas phase reactions*



Water splitting as a method for sustainable (solar) energy storage is realized in biological environments within the photosystem II (PS II). Recent X-ray diffraction investigations at 1.9 Å resolution revealed that the detailed structure of the active water oxidizing center (WOC) of the PS II system consists of a near cubic CaMn_3O_4 unit tethered to a fourth manganese atom through additional oxo bridges.¹ This structural motif has inspired efforts to synthesize biomimetic water splitting catalysts based on ligated bi- or mostly tetra-nuclear manganese-oxo complexes^{2–5} as well as solid manganese oxide materials.⁶

While large research efforts have been invested and progress has been made in understanding the photosynthetic process, the interaction of the WOC with H_2O molecules and the mechanistic details of the actual water splitting reaction remain largely elusive, though several reaction schemes have been proposed.⁷ In particular, facilitation of water oxidation via dynamic structural changes has been emphasized.^{8,9} It is therefore imperative to develop novel suitable model systems, which are simple enough to enable a molecular level insight into the catalytic water splitting process, while capturing some of the essential features of the more complete photosynthetic system. To this aim, size-selected free manganese oxide clusters provide the required simplicity while, at the same time, offering a level of complexity that makes the conclusions and lessons drawn from such model studies relevant to the bottom up design of bioinspired water-splitting molecular catalysts. In particular, they help to gain deeper insights into structure–activity principles operating in the WOC as well as enhanced understanding of the water splitting reaction.

In the present contribution, we explore the mechanistic differences in the water splitting reaction mediated by bi- and tetra-nuclear singly charged manganese oxide clusters, Mn_2O_2^+ and Mn_4O_4^+ , through a combination of first-principles theoretical simulations and ion trap mass spectrometry, revealing the importance of water-induced structural dimensionality changes in these model complexes.

Results and Discussion. At multicollision conditions in the gas-filled ion trap both Mn_2O_2^+ and Mn_4O_4^+ readily react with water to form a series of measured reaction product complexes displayed in Figure 1 and predicted theoretically as shown in Figures 2 and 3.

The interaction of Mn_2O_2^+ with H_2O is depicted in Figure 2, starting from the bare cluster shown at the top of Figure 2a, exhibiting a magnetic moment corresponding to $\mu = 9\mu_B$ (that is, nine unpaired electrons, which is the maximal magnetization of the cluster cation due to the valence d-electrons). In contrast to the Mn_2O_2^+ cluster the neutral Mn_2O_2 cluster is non-magnetic, and formation of the cation entails an ionization, with an adiabatic ionization energy (that is, the difference total energy between the total energy of the ground state parent neutral and the relaxed ionized product cation) of $\text{aIP} = 6.79$ eV. The theoretically simulated lowest energy pathway for the interaction of Mn_2O_2^+ with H_2O (Figure 2a) involves adsorption of water molecules at the Mn atom sites followed by migration of hydrogen atoms to the μ -bridging oxygens of

Received: August 22, 2013

Revised: October 2, 2013

Published: October 28, 2013

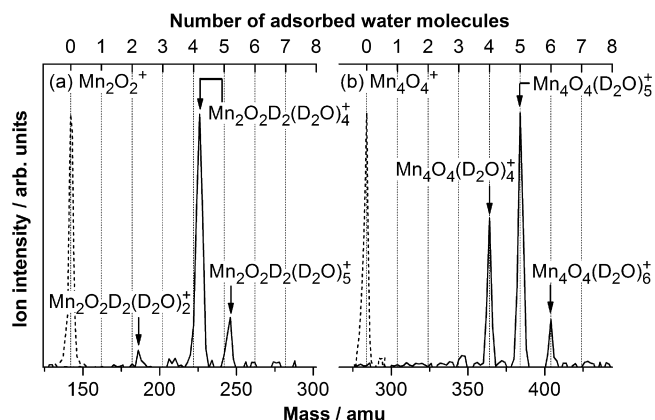


Figure 1. Product ion mass distributions recorded after the reaction of mass selected (a) Mn_2O_2^+ and (b) Mn_4O_4^+ in the ion trap, which was filled with 1.0 Pa of helium and 0.001 Pa of D_2O at room temperature. The dashed signals indicate the mass spectra of the bare manganese oxide clusters before the reaction with water. The reaction time, that is, the storage time in the ion trap, was 0.1 s. The relative product intensities remain unchanged at longer reaction times.

the cluster, resulting in the tetra-hydroxy-complex shown as structure G in Figure 2a. This mechanism is thermodynamically more favorable than the simple adsorption of two water molecules as can be seen from the higher energy of the structures I and J in Figure 2a. Most surprisingly, however, and although it is thermodynamically and kinetically most feasible under the experimental reaction conditions, the mass spectrometrically observed reaction products [see the $\text{Mn}_2\text{O}_2\text{D}_2(\text{D}_2\text{O})_n^+$ ($n = 2, 4, 5$) signals displayed in Figure 1a] indicate the operational dominance of an alternative mechanism. That mechanism would entail hydrogen atom stripping in conjunction with the liberation of the neutral oxidized equivalents.

The elimination of bridging or terminal hydroxyl groups from the tetra-hydroxy-manganese complex, G (or its higher energy isomer H) in Figure 2a, to yield the bis-hydroxy-manganese $\text{Mn}_2\text{O}_2\text{H}_2^+$ complex, is, however, thermodynamically nonfeasible because of the large energy difference. Indeed, our theoretical simulations reveal that the stripping mechanism consists of the concerted formation and release of hydrogen peroxide after dehydrogenation of two water molecules by Mn_2O_2^+ . We find that the exothermicity of the reaction is 0.4 eV, resulting in formation of the bis-hydroxy-manganese complex shown as structure K in Figure 2a along with an H_2O_2 molecule. The observed formation of the intermediate bis-hydroxy-product (K, Figure 2a) in the reaction of Mn_2O_2^+ with water in our multicollision ion trap experiment is in accordance with previous reaction studies performed under single-collision conditions.^{10,11}

The subsequent adsorption of further water molecules onto $\text{Mn}_2\text{O}_2\text{H}_2^+$, as depicted in Figure 2b, has not been studied before and leads to the experimentally observed products $\text{Mn}_2\text{O}_2\text{D}_2(\text{D}_2\text{O})_2^+$, $\text{Mn}_2\text{O}_2\text{D}_2(\text{D}_2\text{O})_4^+$, and $\text{Mn}_2\text{O}_2\text{D}_2(\text{D}_2\text{O})_5^+$ (see Figure 1a) without further change of the general structural motif of $\text{Mn}_2\text{O}_2\text{H}_2^+$. It is nevertheless noteworthy that the adsorption of additional water molecules via hydrogen bonding for some complexes, for example, $\text{Mn}_2\text{O}_2\text{H}_2(\text{H}_2\text{O})_2^+$, appears energetically more favorable than the interaction with the Mn metal atom site (cf. structures M and N in Figure 2b).

Interestingly, the possibility of a reoxidation of the bis-hydroxy-product $\text{Mn}_2\text{O}_2\text{H}_2^+$ to the initial Mn_2O_2^+ cluster by

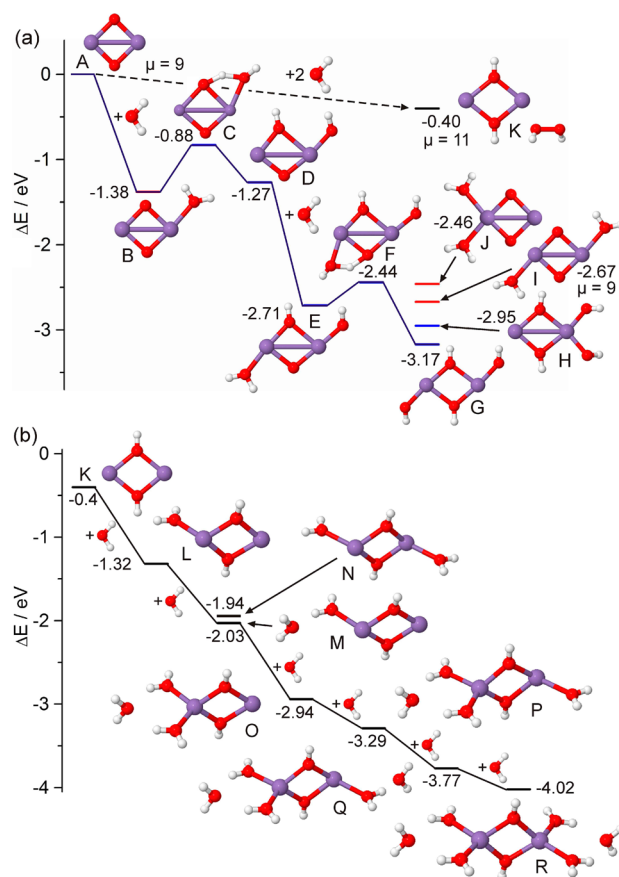
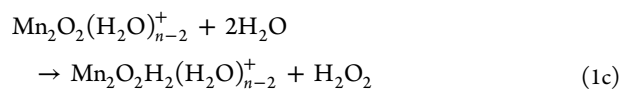
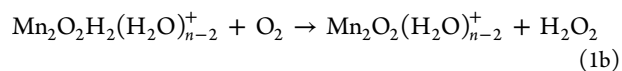


Figure 2. (a) Calculated lowest energy reaction pathway for the interaction of Mn_2O_2^+ with H_2O . The structure of Mn_2O_2^+ is in accordance with collision induced desorption¹⁰ and spectroscopic³⁰ measurements. For geometrical parameters of the optimized neutral and charged Mn_2O_2 clusters, please see the Supporting Information. The final product after the reaction with two H_2O molecules is represented by the tetra-hydroxy-structure G. The experimental data are in favor of the hydrogen peroxide formation mechanism that yields the bis-hydroxy-product K. (b) Adsorption of up to six water molecules onto the bis-hydroxy-product $\text{Mn}_2\text{O}_2\text{H}_2^+$ (K). All energies are given in eV. For selected structures magnetic moments μ are indicated in units of Bohr magnetons; the magnetic moment of the bare cluster cation does not change upon water adsorption. In some instances, higher energy structural isomers are depicted (see, e.g., H, I, and J in a and N in b). Manganese, oxygen and hydrogen atoms are depicted as purple, red, and white spheres, respectively. Lines connecting the indicated energy differences ΔE with respect to the educts are drawn as a guide to the eye.

reaction with molecular oxygen has been demonstrated previously,¹⁰ thus providing evidence for the feasibility of the necessary back-reaction step of a complete catalytic water oxidation cycle:



The prevalence of this catalytic reaction cycle is indeed very likely to occur under thermal reaction conditions in our ion

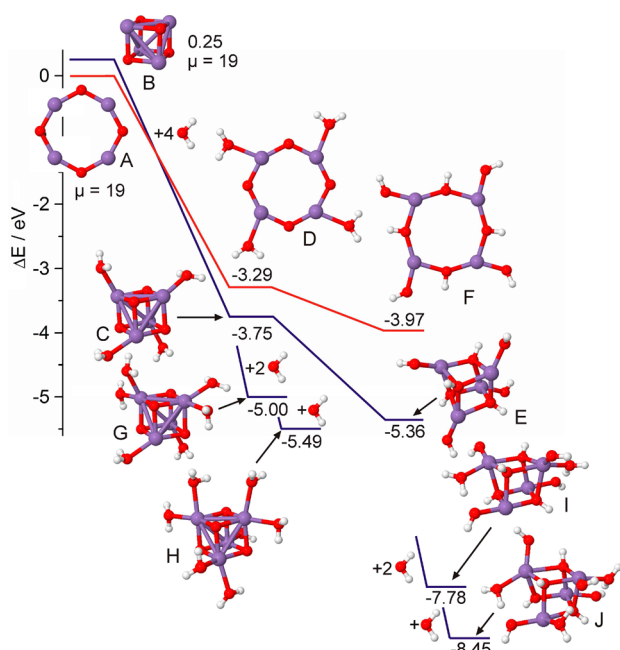


Figure 3. Adsorption of water molecules onto Mn_4O_4^+ , which exhibits a planar 2D lowest energy structure (see A at the top left), causes a dimensionality crossover that favors the cuboidal structure C in the case of the complex $\text{Mn}_4\text{O}_4(\text{H}_2\text{O})_4^+$, observed experimentally; for geometrical parameters of the optimized neutral and charged Mn_4O_4 clusters, see Supporting Information. Water splitting through hydrogen atom migration to μ -bridging oxygen atoms and the formation of an octa-hydroxy-complex E is also considerably more exothermic for the 3D structure C compared to the corresponding 2D structure D; the water splitting process involves an activation barrier smaller than 0.5 eV (that is, smaller than the one for the Mn_2O_2^+ cluster, see Figure 2a). Additional water adsorption results in a further stabilized octa-hydroxy-complex E. All energies are given in eV. For the bare Mn_4O_4^+ isomers magnetic moments μ are indicated in units of Bohr magnetons; the magnetic moment of the bare cluster cation does not change upon water adsorption. The color scheme is as given in Figure 2. Lines connecting the indicated energy differences ΔE with respect to the educts are drawn as a guide to the eye.

trap experiment by introducing both D_2O and O_2 into the ion trap. Yet, it appears that the reoxidation reaction 1b presents the rate determining step, and the resulting $\text{Mn}_2\text{O}_2(\text{D}_2\text{O})_{n-2}^+$ react immediately to form $\text{Mn}_2\text{O}_2\text{D}_2(\text{D}_2\text{O})_{n-2}^+$. Consequently, the mass spectral product intensities observed in Figure 1a do not change significantly upon addition of molecular oxygen to the ion trap.

In marked contrast to Mn_2O_2^+ the tetra-nuclear manganese oxide cluster Mn_4O_4^+ exhibits only reaction products of the stoichiometry $\text{Mn}_4\text{O}_4(\text{D}_2\text{O})_n^+$ after room temperature interaction with water in the ion trap (Figure 1b). Therefore, in this case the theoretically predicted lowest energy reaction mechanism involving the adsorption of water at the Mn atom sites followed by hydrogen migration to the μ -bridging oxygen atoms of the cluster to yield a multiple-hydroxy complex (similar to the prediction for Mn_2O_2^+) would indeed be well in accordance with the experimental observations.

For the neutral Mn_4O_4 cluster we have found through unconstrained Born–Oppenheimer spin-density-functional theory molecular dynamics (BO-SDF-MD) simulations¹² a two-dimensional (2D) ring-like optimal ground state geometry¹³ (non magnetic $\mu = 0$, with nearest neighbor Mn atoms having antiparallel d-electron magnetization). This finding

contrasts previous calculations that have employed biased explorations of the cluster potential energy surface,^{14,15} which predicted a 3D cubic ground state. The neutral cluster possesses also two higher energy isomers: a 3D cubic one with $\Delta E = 0.53$ eV and $\mu = 10$ (with one of the Mn atoms having a d-electron magnetization of opposite direction than the other three Mn atoms), and a 2D, ladder-like, isomer with $\Delta E = 0.78$ eV and $\mu = 20$; see Supporting Information.

The bare Mn_4O_4^+ cluster, which can be obtained from the neutral one upon ionization (aIP = 7.0 eV), was found by us to also have a 2D ground state optimal ring geometry (structure A in Figure 3), with $\mu = 19$ unpaired d electrons (that is, maximal d-electron magnetization); this singly charged 2D cluster possesses a higher energy ($\Delta E = 0.25$ eV) 3D cubic isomer (see Figure 3, structure B) and an even higher energy 2D ladder-like one ($\Delta E = 0.46$ eV), both having $\mu = 19$; see Supporting Information.

The interconversion pathway between the ring (2D) and cube (3D) isomers of Mn_4O_4^+ is depicted in Figure 4a. The

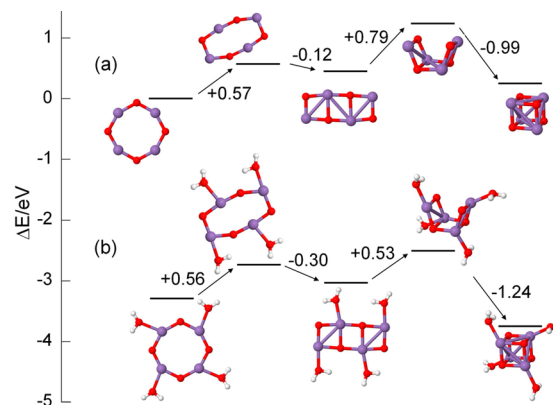


Figure 4. Dimensionality interconversion pathways calculated for the bare (a) and hydrated (b) Mn_4O_4^+ cluster. (a) The structural transformation of the bare cluster starts from the 2D ring-like isomer (leftmost configuration) and ends with the 3D cuboidal structure depicted on the right. Two TS activation barriers are encountered (0.57 and 0.79 eV) with an intermediate (local minimum) ladder-like configuration (third one from the left). (b) The same as a but for the hydrated $\text{Mn}_4\text{O}_4(\text{H}_2\text{O})_4^+$ cluster. The two TS barriers are 0.56 and 0.53 eV. In both a and b, the energy of the initial configuration (2D ring-like isomer) is taken as the zero of the energy scale. Mn atoms are depicted by larger purple spheres, and oxygen atoms are depicted by small red spheres. H atoms are represented by smaller white spheres.

transformation involves two transition state (TS) activation barriers: (1) the first one ($\Delta E_a^{(1)} = 0.57$ eV) leads to a local-minimum intermediate with a 2D ladder configuration, having an energy of 0.46 eV higher than that of the ground state (ring) isomer; (2) The second barrier ($\Delta E_a^{(2)} = 0.79$ eV) corresponds to “folding” of the ladder culminating in the 3D (cube) isomer (rightmost configuration in Figure 4a). The higher (second) TS barrier, and the higher energy of the final state with reference to the starting 2D isomer, indicate that such a dimensionality crossover may occur for the bare cluster only at higher temperatures.

The energy balance between the 2D and 3D isomers of the cluster varies upon the interaction of the cluster with water. The 2D structure remains favored after the adsorption of a single water molecule; that is, the energy of the 2D, ring, isomer of $\text{Mn}_4\text{O}_4(\text{H}_2\text{O})^+$, calculated with reference to the correspond-

ing bare cluster, is $\delta E = -0.93$ eV, compared to $\delta E = -0.79$ eV calculated for the cube isomer; this results in an energy of $\delta E(2D/3D) = 0.14$ eV in favor of the lower dimensionality cluster. While the energies of the 2D and 3D dihydrated clusters, $\text{Mn}_4\text{O}_4(\text{H}_2\text{O})_2^+$, are essentially the same (i.e., $\delta E(2D) = -1.82$ eV, and $\delta E(3D) = -1.83$ eV), the balance tilts in favor of the higher dimensionality cluster for a larger number of adsorbed water molecules: that is, for $\text{Mn}_4\text{O}_4(\text{H}_2\text{O})_3^+$, $\delta E(2D) = -2.63$ eV, and $\delta E(3D) = -2.84$ eV), resulting in $\delta E(2D/3D) = 0.21$ eV in favor of the higher dimensionality (3D) cluster, and for $\text{Mn}_4\text{O}_4(\text{H}_2\text{O})_4^+$, $\delta E(2D) = -3.29$ eV, and $\delta E(3D) = -3.75$ eV, resulting in an even larger energy advantage ($\delta E(2D/3D) = 0.46$ eV) favoring the 3D hydrated cube-like isomer. Consequently, we predict that the adsorption of water molecules brings about a dimensionality crossover where, for $n \geq 2$ adsorbed H_2O molecules, the 2D ring of Mn_4O_4^+ is transformed into a 3D cubic Mn_4O_4^+ core with $n\text{H}_2\text{O}$ bound to the Mn atom vertices via the oxygen as the lowest energy structure of the complex $\text{Mn}_4\text{O}_4(\text{H}_2\text{O})_n^+$ (for $n = 4$ see structure C in Figure 3).

In Figure 4b we display the dimensionality crossover mechanism for the case of $\text{Mn}_4\text{O}_4(\text{H}_2\text{O})_4^+$, starting from the 2D ring isomer (leftmost configuration). The mechanism is similar to that found for the bare cluster (Figure 4a), with the principal difference being: (i) The deeper local minimum of the hydrated ladder isomer (-0.3 eV with respect to the first TS $\Delta E_a^{(1)} = 0.56$ eV); (ii) the significantly lower barrier of the second TS activation barrier ($\Delta E_a^{(2)} = 0.53$ eV), and (iii) the 3D hydrated cube product is lower in energy than the initial state (-0.46 eV). The stabilization of the ladder intermediate (lowering the rate of back conversion to the ring isomer), the lowering of the second TS activation energy, and the enthalpic energy balance favoring the product isomer lead us to conclude that the 2D-to-3D dimensionality crossover is likely to occur upon hydration of the tetraoxide manganese cluster cation.

The change in dimensionality from the 2D ring structure of the free cluster to the 3D cuboidal structure of Mn_4O_4^+ in the water complex facilitates considerably the activation of one O–H bond in each water molecule. Indeed, for the ring isomer of $\text{Mn}_4\text{O}_4(\text{H}_2\text{O})_4^+$ we find a dissociation activation barrier $\Delta E_D^{(1)} = 0.15$ eV for the first H_2O dissociation, and consecutive dissociation of a second molecule entails a slightly larger barrier $\Delta E_D^{(2)} = 0.21$ eV, while for the cube isomer of the cluster the first dissociation is calculated to be essentially barrierless (i.e., $\Delta E_D^{(1)} < 0.05$ eV), and dissociation of the second molecule entails an even smaller barrier ($\Delta E_D^{(1)} = 0.03$ eV). Room temperature 2.5 ps FPBOMD simulations (see Methods section) of the $\text{Mn}_4\text{O}_4(\text{H}_2\text{O})_4^+$ cluster have revealed splitting (dissociation) of two of the adsorbed molecules (with the first occurring after 2.25 ps and the second taking place shortly after) resulting in a partially hydroxylated cluster.

The subsequent hydrogen migration to the μ -oxo bridges is significantly more exothermic (by 0.93 eV) for the cuboidal structure (reaction C \rightarrow E, Figure 3) compared to the ring structure complex (reaction D \rightarrow F, Figure 3). Hence, it can be concluded that water adsorption determines the (3D) dimensionality of the Mn_4O_4^+ cluster unit and the favored cuboidal geometry, which resembles the WOC geometry in PSII. This, in turn, promotes the water splitting and hydrogen atom transfer reaction representing the first step toward water oxidation to O_2 .

Ligated $\text{Mn}_4\text{O}_4^{6+}$ cubane core structures have been prepared in solution, and it has been demonstrated that the cuboidal core

topology—in marked contrast to bis-manganese complexes—is structurally suited for water oxidation and O_2 release. High-yield O_2 formation has indeed been detected after laser excitation of ligated $\text{Mn}_4\text{O}_4^{6+}$ cubane core structures in gas phase experiments.^{5,16}

Further water adsorption onto the complexes C and E have also been calculated and are displayed in Figure 3 illustrating that a 3D tetra-hydroxy- Mn_4O_4^+ -complex structure can be most likely assigned to all experimentally observed stoichiometries $\text{Mn}_4\text{O}_4(\text{D}_2\text{O})_{4-6}^+$ (cf. Figure 1b).

Structural properties of the manganese oxide clusters discussed above could be explored with the use of vibrational spectroscopy which is inherently sensitive to the cluster dimensionality, structure, and nature of bonding of adsorbed species. Far-infrared multiple-photon dissociation (FIR-MPD) spectroscopy is a technique that has been proven to be most useful for obtaining vibrational spectra of gas phase clusters.^{17–20} This technique in conjunction with calculated vibrational spectra (using first-principle theories) allows the determination of structural parameters of the cluster system through comparisons between the measured and calculated spectra. In anticipation of such measurements we give below details of vibrational spectra calculated for the systems studied here.

The ground state 2D ring structure and the higher energy 3D cuboidal isomer of the bare Mn_4O_4^+ cluster can be distinguished by comparing the vibrational spectra shown in Figure 5a and b. It is also evident that the vibrations of the 2D isomer extend to higher frequencies than those of the 3D cluster; see the set of peaks above 600 cm^{-1} in Figure 5a corresponding to vibrations (mainly of the lighter mass, oxygen atoms) along the Mn–O bonds of the ring (see Figure S4a). For values of all the calculated normal-mode frequencies see the Supporting Information; because of numerical inaccuracies at low frequencies, we focus on vibrational modes with $\nu > 100\text{ cm}^{-1}$, which we estimate to be quantitatively reliable.

Upon adsorption of water the hydrated cluster exhibits distinctly different vibrational spectra (VS) for the tetra-water $\text{Mn}_4\text{O}_4(\text{H}_2\text{O})_4^+$ (undissociated water molecules) adsorption complex (Figure 5c) and the cuboidal octa-hydroxy-complex $(\text{MnOH})_4(\text{OH})_4^+$ (Figure 5d). For both cases the insets show the VS in an extended frequency range. For the nondissociative water adsorption in Figure 5c the high energy vibrations with $\nu_s = 3721\text{--}3737\text{ cm}^{-1}$ and $\nu_{as} = 3513\text{--}3614\text{ cm}^{-1}$ correspond, respectively, to the symmetric and asymmetric OH vibrational modes, those at $\nu_b = 1550\text{--}1577\text{ cm}^{-1}$ are HOH bending modes, and the ones with $\nu = 500\text{--}600\text{ cm}^{-1}$ correspond to librations/rotations of the adsorbed water molecules; in the gas phase the vibrations of the H_2O molecule are characterized by the following (measured) frequencies²¹ $\nu_s = 3759.4\text{ cm}^{-1}$, $\nu_{as} = 3649.6\text{ cm}^{-1}$, and $\nu_b = 1375.5\text{ cm}^{-1}$. The water bending vibrational mode disappears upon dissociation (splitting) of the adsorbed molecule leading to formation of the cuboidal octa-hydroxy-complex (see inset in Figure 5d). Furthermore, in Figure 5c and d we distinguish between the total vibrational spectra (including all atoms of the hydrated tetra-manganese-oxide cluster) represented by the red color curves and the projected vibrational spectra (PVS) shown in blue color which include vibrational displacements of only the atoms of the parent Mn_4O_4^+ cluster; the difference between the two curves gives the contribution of the vibrational motions of the adsorbed hydrous species.

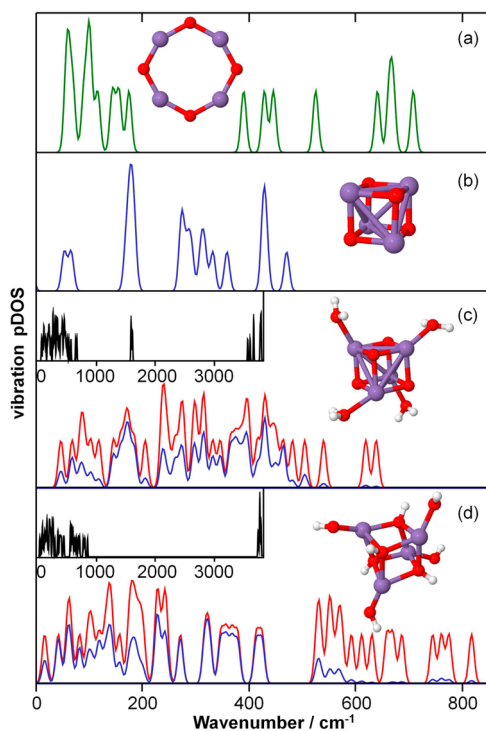


Figure 5. Calculated vibrational spectra (VS) of bare and hydrated Mn_4O_4^+ clusters (for a listing of the vibrational mode frequencies see the Supporting Information). (a) VS of the 2D ring isomer of bare Mn_4O_4^+ . The highest vibrational frequencies $\nu > 600 \text{ cm}^{-1}$ correspond to in-plane displacements of an O atom to-and-fro the nearest neighbor Mn atoms (see Figure S4a), and the $\nu < 200 \text{ cm}^{-1}$ frequencies correspond to out of plane vibrations of the oxygen atoms. In the mode at $\nu = 360 \text{ cm}^{-1}$ the Mn and O atoms displace in the plane, with both oxygens on the up–down (north–south) diagonal moving inward, and the oxygens on the horizontal (east–west diagonal) displacing outward; at the same time the two Mn atoms located above the horizontal diagonal move toward the top oxygen atom, and those located below the horizontal diagonal move toward the bottom oxygen. (b) VS of the higher-energy 3D cuboidal isomer of bare Mn_4O_4^+ . In the modes corresponding to the highest frequencies, $\nu \sim 470 \text{ cm}^{-1}$, the Mn and O atoms connected by the cube diagonal both move in or out (breathing mode) with respect to the center of the cube (Figure S4b). The mode at 273 cm^{-1} corresponds to displacements in opposite directions of the Mn and O atoms (e.g. Mn toward the cube center, and the corresponding O moves away from the center) along the cube diagonals. Modes in the $\nu = 165\text{--}180 \text{ cm}^{-1}$ range appear to be twisting and/or shearing modes of the cube. (c) VS of the cuboidal tetra-water-complex $\text{Mn}_4\text{O}_4(\text{H}_2\text{O})_4^+$, with the vibrational modes of the adsorbed molecules described in the text. (d) VS of the 3D octa-hydroxy-complex, $(\text{MnOH})_4(\text{OH})_4^+$, resulting from splitting of the water molecules. Here modes with $\nu = 3680\text{--}3734 \text{ cm}^{-1}$ correspond to adsorbed OH stretch vibrations, and modes with $\nu = 746\text{--}819 \text{ cm}^{-1}$ correspond to librations of the OH groups at the cube corners (oxygen sites with three Mn nearest neighbors, Figure S4d); librations of the other four OH groups (each bonded directly to an Mn atom) are characterized by $\nu \sim 600\text{--}700 \text{ cm}^{-1}$, and $\nu = 530\text{--}600 \text{ cm}^{-1}$ corresponds to stretch displacement of the Mn–OH bond (Figure S4d). In c and d, the red spectra represent the total vibrational density of states (DOS), while the projected VS (PVS), corresponding to contributions only of the Mn_4O_4^+ cluster core atoms, are depicted in blue. The insets in c and d display spectral views in an extended wavenumber range. In the structural models, red spheres represent O atoms, purple spheres correspond to Mn atoms, and hydrogen atoms are in white.

An examination of the vibrational spectra in Figure 5 leads us to conclude that the structural dimensionality crossover as well as the concurrent hydrogen migration to the μ -oxo bridges should be readily observable in the infrared absorption characteristics of the cluster complexes.

We note here that, while our focus in the present contribution is on the reactions of the cationic tetra-manganese oxide cluster, our calculations for the neutral Mn_4O_4 cluster show water adsorption accompanied by a 2D-to-3D dimensionality transformation, water splitting, and hydrogen migration resulting in a cuboidal octa-hydroxy-complex similar to that described above for the cluster cation.

Conclusion. In summary, we have focused here on joint gas phase ion-trap experiments and first-principles theoretical investigations of the interaction of ligand-free manganese oxide clusters with water, aiming at a bottom-up approach toward the design of bioinspired artificial water-splitting molecular catalysts. Although the mechanistic details of water splitting at the WOC remain a matter of intense investigations, the essential functions of the WOC, pertaining to binding and activating water as well as delocalization of oxidizing equivalents upon hydrogen atom stripping,^{7,10,16} are well-recognized. Our gas phase reactivity studies and first-principles simulations of ligand-free mass-selected Mn_2O_2^+ and Mn_4O_4^+ complexes offer new insight into the mechanism of this process and demonstrate the importance of the water adsorption induced dimensionality change of Mn_4O_4^+ that is essential to the formation of the cuboidal core structure that facilitates hydrogen abstraction and possibly eventually light-induced oxygen evolution. This final reaction step is currently under investigation in our laboratories.

We have also presented first-principles theoretically calculated vibrational spectra that have been found to portray variations in dimensionality and structure of the charged manganese tetraoxide cluster upon interaction with water, as well as spectral changes that accompany water splitting and hydrogen migration to the μ -oxo bridges. These predictions provide the impetus for future measurements with FIR-MPD spectroscopy.

Methods. Experimental Methods. Ligand-free gas phase manganese oxide clusters are prepared by sputtering of preoxidized Mn metal targets with high energy Xe ion beams. This approach allows for the controlled preparation of stoichiometric $(\text{MnO})_n^+$. Previously, stoichiometric cationic²² or oxygen-rich anionic^{11,23–25} manganese oxide cluster distributions have been prepared using laser ablation techniques. The produced clusters are mass selected in a first quadrupole mass filter and are subsequently guided into the home-built radio frequency octopole ion trap, which is prefilled with 1 Pa of helium buffer gas and a small partial pressure of water. The pressure conditions ensure temperature equilibration of the clusters within a few milliseconds prior to the reaction with water which occurs on a considerably longer time scale.²⁶ During the experiments the ion trap is held at room temperature, and after a chosen reaction time, that is, storage time inside the ion trap, all ions, products and intermediates, are extracted and mass analyzed by a second quadrupole mass filter and finally detected with a channeltron amplifier. Throughout the presented experiments deuterated water was employed to facilitate the mass assignment.

Theoretical Methods. The theoretical explorations of the atomic arrangements and electronic structures of the manganese oxide clusters and their complexes were performed

with the use of the BO-SDF-MD¹² with norm-conserving soft (scalar relativistic for Mn) pseudopotentials²⁷ and the generalized gradient approximation (GGA)²⁸ for electronic exchange and correlations. In these calculations we have used a plane-wave basis with a kinetic energy cutoff $E_c = 62$ Ry, which yields convergence. This corresponds to a real-space grid spacing of $0.4a_0$ (Bohr radius); the real-space grid spacing for the density (and potential) was $0.133a_0$ corresponding to $E_c = 555$ Ry. In the construction of the Mn pseudopotentials the valence electrons, $3d^5$ and $4s^2$, were characterized by core radii $r_c(s) = 2.35a_0$ and $r_c(d) = 2.35a_0$, with the s orbital treated as local. For the oxygen atom pseudopotential the valence $2s^2$ and $2p^4$ electrons were treated with $r_c(s) = r_c(p) = 1.45a_0$, with the p orbital treated as local. The BO-SDF-MD method is particularly suitable for investigations of charged systems since it does not employ a supercell (i.e., no periodic replication of the ionic system is used). In all of the calculations the dependence on spin multiplicity has been checked, and the results that we report correspond to the spin multiplicities with the lowest energies. The energy minimization to find the optimal cluster geometry was done with a steepest-descent method. The convergence criteria was that the maximum force magnitude on any particle is less than 0.0005 hartree/bohr and that the average over all particles is less than 0.00025 hartree/bohr. First principles Born–Oppenheimer molecular dynamics (FPBOMD) simulations of typically a few picosecond duration at 300 K (that is, canonical, constant temperature, simulations, with stochastic thermalization) were used to ensure that the resulting optimal configurations were stable; a time-step of 0.25 fs was used in these simulations. For the clusters with adsorbed water longer runs were used to explore configuration space and suggest starting geometries for the minimization. In addition FPBOMD simulations were used to explore the water splitting process on the $\text{Mn}_4\text{O}_4(\text{H}_2\text{O})_4^+$ cluster.

In the first-principles calculations of the reaction profiles (pathways) shown in Figure 2, a reaction coordinate was judiciously chosen. Typically, the reaction coordinate consists of the distance between two atoms of the reactant molecules; see for example calculations of transition state barriers calculated for the interaction of Mn_2O_2^+ with H_2O and depicted in Figure 2a, where the distance of an H atom of an adsorbed water molecule and the μ -oxo bridge has been used as a reaction coordinate. Alternatively, in calculations of the dissociation barriers of water molecules adsorbed on the 2D and 3D isomers of $\text{Mn}_4\text{O}_4(\text{H}_2\text{O})_4^+$ we have used as a reaction coordinate the ratio of the distance $d(\text{O}-\text{H}_\text{D})$ between the dissociating H_D atom and the O atom of the HOH_D molecule involved in the water splitting process, and the distance $d(\text{H}_\text{D}-\text{O})$ between H_D and the neighboring O atoms of the manganese tetra-oxide cluster; for the reaction coordinates used in the calculations of the 2D-to-3D dimensionality conversion pathways depicted in Figure 4, see Supporting Information. For each value of the reaction coordinate, the total energy of the system was optimized through unconstrained relaxation of all of the other degrees of freedom of the system. The reaction profiles (reaction paths) were obtained via repeating such calculations for various values of the chosen reaction coordinate; once the top of the transition state activation barrier is achieved, the incremented variation of the reaction coordinate is stopped, and the system is allowed to relax freely into the product well. These calculations yield results that are the same as, or close to, those obtained by other

methods, for example, the nudged elastic band and variants thereof; see the discussion on pp 89 and 90 in ref 29.

In the calculation of the vibration spectrum the dynamical matrix was constructed from the finite difference of forces on each atom when an atom is displaced along the Cartesian directions. For each displacement the electronic structure is converged using a real-space grid with a small spacing of $0.1a_0$ to reduce grid effects. Averaging of the results from four displacements of $\pm 0.015a_0$ and $\pm 0.03a_0$ further adds to the accuracy of the results. The projected vibrational spectrum (PVS) is obtained by multiplying (weighting) the total vibrational density of states at the normal-mode frequency ν_l by the sum of the squares of the coefficients of the displacements of a subset of atoms (in Figure 5c and d the atoms of the parent Mn_4O_4^+ cluster) in the corresponding (normalized) normal mode eigenvector $\mathbf{v}(\nu_l)$. In plots of the vibrational spectrum we used the results of convoluting the frequencies (delta-functions) with a Gaussian of width 10 cm^{-1} .

■ ASSOCIATED CONTENT

Supporting Information

Details of the geometric data. This material is available free of charge via the Internet at <http://pubs.acs.org>.

■ AUTHOR INFORMATION

Corresponding Authors

*E-mail: thorsten.bernhardt@uni-ulm.de.

*E-mail: uzi.landman@physics.gatech.edu.

Notes

The authors declare no competing financial interest.

■ ACKNOWLEDGMENTS

This work was supported by the DFG. S.M.L. is grateful to the ESF Baden-Württemberg for a Margarete von Wrangell fellowship. The work of R.N.B. at the Georgia Institute of Technology was supported by a grant from the U.S. Air Force Office of Scientific Research, and the work of U.L. was supported in part by a grant from the Office of Basic Energy Sciences of the U.S. Department of Energy under contract no. FG05-86ER45234. Calculations were performed at the Georgia Institute of Technology Center for Computational Materials Science.

■ REFERENCES

- (1) Umena, Y.; Kawakami, K.; Shen, J.-R.; Kamiya, N. Crystal Structure of Oxygen-Evolving Photosystem II at a Resolution of 1.9 Å. *Nature* **2011**, *473*, 55–60.
- (2) Yagi, M.; Kaneko, M. Molecular Catalysts for Water Oxidation. *Chem. Rev.* **2001**, *101*, 21–36.
- (3) Mukhopadhyay, S.; Mandal, S. K.; Bhaduri, S.; Armstrong, W. H. Manganese Clusters with Relevance to Photosystem II. *Chem. Rev.* **2004**, *104*, 3981–4026.
- (4) Brimblecombe, R.; Swiegers, G. F.; Dismukes, G. C.; Spiccia, L. Sustained Water Oxidation Photocatalysis by a Bioinspired Manganese Cluster. *Angew. Chem., Int. Ed.* **2008**, *47*, 7335.
- (5) Dismukes, G. C.; Brimblecombe, R.; Felton, G. A. N.; Pryadun, R. S.; Sheats, J. E.; Spiccia, L.; Swiegers, G. F. Development of Bioinspired Mn_4O_4 -Cubane Water Oxidation Catalysts: Lessons from Photosynthesis. *Acc. Chem. Res.* **2009**, *42*, 1935–1943.
- (6) Najafpour, M. M.; Ehrenberg, T.; Wiechen, M.; Kurz, P. Calcium Manganese(III) Oxides ($\text{CaMn}_2\text{O}_4 \cdot x\text{H}_2\text{O}$) as Biomimetic Oxygen-Evolving Catalysts. *Angew. Chem., Int. Ed.* **2010**, *49*, 2233–2237.
- (7) Dau, H.; Limberg, C.; Reier, T.; Risch, M.; Roggan, S.; Strasser, P. The Mechanism of Water Oxidation: From Electrolysis via

Homogeneous to Biological Catalysis. *Chem. Cat. Chem.* **2010**, *2*, 724–761.

(8) Haumann, M.; Müller, C.; Liebisch, P.; Iuzzolino, L.; Dittmer, J.; Garbolle, M.; Neisius, T.; Meyer-Klaucke, W.; Dau, H. Structural and Oxidation State Changes of the Photosystem II Manganese Complex in Four Transitions of the Water Oxidation Cycle ($S_0 \rightarrow S_1$, $S_1 \rightarrow S_2$, $S_2 \rightarrow S_3$, and $S_{3,4} \rightarrow S_0$) Characterized by X-ray Absorption Spectroscopy at 20 K and Room Temperature. *Biochemistry* **2005**, *44*, 1894–1908.

(9) Klauss, A.; Sikora, T.; Süß, B.; Dau, H. Fast Structural Changes (200–900 ns) May Prepare the Photosynthetic Manganese Complex for Oxidation by the Adjacent Tyrosine Radical. *Biochim. Biophys. Acta—Bioenergetics* **2012**, *1817*, 1196–1207.

(10) Chiavarino, B.; Crestoni, M. E.; Fornarini, S. Gas-Phase Dioxygen Activation by Binuclear Manganese Clusters. *Chem.—Eur. J.* **2002**, *8*, 2740–2746.

(11) Oliveira, M. C.; Marcalo, J.; Vieira, M. C.; Almoester Ferreira, M. A. Formation of Some Transition Metal Oxide Cluster Anions and Reactivity Towards Methanol in the Gas Phase. *Int. J. Mass Spectrom.* **1999**, *185–187*, 825–835.

(12) Barnett, R. N.; Landman, U. Born-Oppenheimer Molecular Dynamics Simulations of Finite Systems: Structure and Dynamics of $(H_2O)_2$. *Phys. Rev. B* **1993**, *48*, 2081–2097.

(13) Ganguly, S.; Kabir, M.; Sanyal, B.; Mookerjee, A. Unusual Structure and Magnetism in Manganese Oxide Nanoclusters. *Phys. Rev. B* **2011**, *83*, 020411.

(14) Nayak, S. K.; Jena, P. Giant Magnetic Moments and Magnetic Bistability of Stoichiometric MnO Clusters. *Phys. Rev. Lett.* **1998**, *81*, 2970–2973.

(15) Nayak, S. K.; Jena, P. Equilibrium Geometry, Stability, and Magnetic Properties of Small MnO Clusters. *J. Am. Chem. Soc.* **1999**, *121*, 644–652.

(16) Ruettinger, W.; Yagi, M.; Wolf, K.; Bernasek, S.; Dismukes, G. C. O_2 Evolution from the Manganese-Oxo Cubane Core $Mn_4O_4^{6+}$: A Molecular Mimic of the Photosynthetic Water Oxidation Enzyme? *J. Am. Chem. Soc.* **2000**, *122*, 10353–10357.

(17) Oomens, J.; Sartakov, B. G.; Meijer, G.; von Helden, G. Gas-Phase Infrared Multiple Photon Dissociation Spectroscopy of Mass-Selected Molecular Ions. *Int. J. Mass Spectrom.* **2006**, *254*, 1–19.

(18) Fielicke, A.; Kirilyuk, A.; Ratsch, C.; Behler, J.; Scheffler, M.; von Helden, G.; Meijer, G. Structure Determination of Isolated Metal Clusters via Far-Infrared Spectroscopy. *Phys. Rev. Lett.* **2004**, *93*, 023401.

(19) Fielicke, A.; von Helden, G.; Meijer, G. Far-Infrared Spectroscopy of Isolated Transition Metal Clusters. *Eur. Phys. J. D* **2005**, *34*, 83–88.

(20) Gruene, P.; Rayner, D. M.; Redlich, B.; van der Meer, A. F. G.; Lyon, J. T.; Meijer, G.; Fielicke, A. Structures of Neutral Au_7 , Au_{19} , and Au_{20} Clusters in the Gas Phase. *Science* **2008**, *321*, 674–676.

(21) Herzberg, G. *Molecular Spectra and Molecular Structure II. Infrared and Raman Spectra of Polyatomic Molecules*; Van Nostrand: Princeton, 1945.

(22) Ziemann, P. J.; Castleman, A. W., Jr. Mass-Spectrometric Investigation of the Stabilities and Structures of Mn-O and Mn-Mg-O Clusters. *Phys. Rev. B* **1992**, *1992*, 13480–13486.

(23) Pramann, A.; Rademann, K. Mass-Spectrometric Study of Formation and Stability of Manganese and Manganese Oxide Cluster Anions. *Int. J. Mass Spectrom.* **1999**, *185–187*, 673–683.

(24) Williams, K. S.; Hooper, J. P.; Horn, J. M.; Lightstone, J. M.; Wang, H.; Ko, Y. J.; Bowen, K. H. Magnetic Structure Variation in Manganese-Oxide Clusters. *J. Chem. Phys.* **2012**, *136*, 134315.

(25) Jia, M.-Y.; Xu, B.; Ding, X.-L.; He, S.-G.; Ge, M.-F. Experimental and Theoretical Study of the Reactions between Manganese Oxide Cluster Anions and Hydrogen Sulfide. *J. Phys. Chem. C* **2012**, *116*, 24184–24192.

(26) Bernhardt, T. M. Gas-Phase Kinetics and Catalytic Reactions of Small Silver and Gold Clusters. *Int. J. Mass Spectrom.* **2005**, *243*, 1–29.

(27) Troullier, N.; Martins, J. L. Efficient Pseudopotentials for Plane-Wave Calculations. *Phys. Rev. B* **1991**, *43*, 1993–2006.

(28) Perdew, J. P.; Burke, K.; Ernzerhof, M. Generalized Gradient Approximation Made Simple. *Phys. Rev. Lett.* **1996**, *77*, 3865–3868.

(29) Bernhardt, T. M.; Heiz, U.; Landman, U. Chemical and Catalytic Properties of Size-Selected Free and Supported Clusters. In *Nanocatalysis*; Heiz, U., Landman, U., Eds.; Springer-Verlag: Berlin, 2007; pp 1–191.

(30) Gong, Y.; Wang, G.; Zhou, M. Formation and Characterization of Mononuclear and Dinuclear Manganese Oxide-Dioxygen Complexes in Solid Argon. *J. Phys. Chem. A* **2008**, *112*, 4936–4941.